

# A Scaler-Based Data Acquisition System for Measuring Parity Violation Asymmetry in Deep Inelastic Scattering

R. Subedi<sup>a,1</sup>, D. Wang<sup>a</sup>, K. Pan<sup>b</sup>, X. Deng<sup>a</sup>, R. Michaels<sup>c</sup>,  
P. E. Reimer<sup>d</sup>, A. Shahinyan<sup>e</sup>, B. Wojtsekhowski<sup>c</sup>, X. Zheng<sup>a,\*</sup>

<sup>a</sup>University of Virginia, Charlottesville, VA 22904, USA

<sup>b</sup>Massachusetts Institute of Technology, Cambridge, MA 02139, USA

<sup>c</sup>Thomas Jefferson National Accelerator Facility, Newport News, VA 23606, USA

<sup>d</sup>Physics Division, Argonne National Laboratory, Argonne, IL 60439, USA

<sup>e</sup>Yerevan Physics Institute, Yerevan 0036, Armenia

---

## Abstract

An experiment that measured the parity violating asymmetries in deep inelastic scattering was completed at the Thomas Jefferson National Accelerator Facility in experimental Hall A. From these asymmetries, a combination of the quark weak axial charge could be extracted with a factor of five improvement in precision over world data. To achieve this, asymmetries at the  $10^{-4}$  level needed to be measured at event rates up to 500 kHz and the high pion background typical to deep inelastic scattering experiments needed to be rejected efficiently. A specialized data acquisition (DAQ) system with intrinsic particle identification (PID) was successfully developed and used: The pion contamination in the electron samples was controlled at the order of  $2 \times 10^{-4}$  or below with an electron efficiency of higher than 91% throughout the production period of the experiment, the systematic uncertainty in the measured asymmetry due to DAQ deadtime was below 0.2%, and the statistical quality of the asymmetry measurement agreed with the Gaussian distribution to over five orders of magnitudes. The DAQ system is presented here with an emphasis on its design scheme, the achieved PID performance, deadtime effect and the capability of measuring small asymmetries.

*Key words:* Jefferson Lab; Hall A; PVDIS; DAQ

*PACS:* 11.30.Er, 12.15.Mm, 13.60.Hb 14.60.Cd 14.65.Bt 29.30.Aj 29.85.Ca

---

<sup>1</sup> Present address: George Washington University, 725 21<sup>st</sup> St, NW, Washington, DC 20052, USA

\* Corresponding author. E-mail: xiaochao@jlab.org; Telephone: 001-434-243-4032; Fax: 001-434-924-4576

29 **1 Introduction**

30 The Parity Violating Deep Inelastic Scattering (PVDIS) experiment E08-011 was  
 31 completed in December 2009 at the Thomas Jefferson National Accelerator Facil-  
 32 ity (JLab). The goal of this experiment [1,2,3] was to measure with high precision  
 33 the parity violating asymmetry in deep inelastic scattering of a polarized 6 GeV  
 34 electron beam on an unpolarized liquid deuterium target. This asymmetry is sensi-  
 35 tive to the quark weak axial charge  $C_{2q}$  which corresponds to a helicity dependence  
 36 in the quark coupling with the  $Z^0$  boson.

37 For electron inclusive scattering from an unpolarized target, the electromagnetic  
 38 interaction is parity conserving and is insensitive to the spin flip of the incom-  
 39 ing electron beam. Only the weak interaction violates parity and causes a differ-  
 40 ence between the right- and the left-handed electron scattering cross-sections  $\sigma_R$   
 41 and  $\sigma_L$ . The dominant contribution to the parity violation asymmetry,  $A_{PV} \equiv$   
 42  $(\sigma_R - \sigma_L)/(\sigma_R + \sigma_L)$ , arises from the interference between electromagnetic and  
 43 weak interactions and is proportional to the four momentum transfer squared  $Q^2$   
 44 for  $Q^2 \ll M_Z^2$ . The magnitude of the asymmetry is on the order of  $10^{-4}$  or  $10^2$  parts  
 45 per million (ppm) at  $Q^2 = 1$  (GeV/c) $^2$ .

46 The PVDIS asymmetry from a deuterium target is

$$A_{PV} = \left( -\frac{G_F Q^2}{4\sqrt{2}\pi\alpha} \right) \left( 2g_A^e Y_1 \frac{F_1^{\gamma Z}}{F_1^\gamma} + g_V^e Y_3 \frac{F_3^{\gamma Z}}{F_1^\gamma} \right), \quad (1)$$

47 where  $Q^2$  is the negative of the four-momentum transfer squared,  $G_F$  is the Fermi  
 48 weak coupling constant,  $\alpha$  is the fine structure constant,  $Y_1$  and  $Y_3$  are kinematic  
 49 factors,  $x$  is the Bjorken scaling variable, and  $F_{1,3}^{\gamma(Z)}$  are deuteron structure functions  
 50 that can be evaluated from the parton distribution functions and the quark- $Z^0$  vector  
 51 and axial couplings  $g_{V,A}^q$ . From this asymmetry one can extract the quark weak  
 52 vector and axial charges  $C_{1,2q}$ , where the quark weak vector charge is defined as  
 53  $C_{1q} \equiv 2g_A^e g_V^q$  and the quark weak axial charge is given by  $C_{2q} \equiv 2g_V^e g_A^q$  with  $q =$   
 54  $u, d$  indicating an up or a down quark,  $g_{A(V)}^e$  is the electron axial (vector) coupling  
 55 and  $g_{V(A)}^q$  is the quark vector (axial) coupling to the  $Z^0$  boson. In the tree-level  
 56 Standard Model, the  $C_{1,2q}$  are related to the weak mixing angle  $\theta_W$ :  $C_{1u} = -\frac{1}{2} +$   
 57  $\frac{3}{4} \sin^2 \theta_W$ ,  $C_{2u} = -\frac{1}{2} + 2 \sin^2 \theta_W$ ,  $C_{1d} = \frac{1}{2} - \frac{2}{3} \sin^2 \theta_W$ , and  $C_{2d} = \frac{1}{2} - 2 \sin^2 \theta_W$ .  
 58 Although the weak mixing angle and the quark weak vector charge  $C_{1q}$  have been  
 59 measured from various processes [4], the current knowledge of the quark weak  
 60 axial charge  $C_{2q}$  is poor and their deviations from the Standard Model value would  
 61 reveal possible New Physics in the quark axial couplings that could not be accessed  
 62 from other Standard Model parameters.

63 The goal of JLab E08-011 was to measure the PVDIS asymmetries to statistical

64 precisions of 3% and 4% at  $Q^2 = 1.1$  and  $1.9$  (GeV/c)<sup>2</sup>, respectively, and under the  
 65 assumption that hadronic physics corrections are small, to extract the quark axial  
 66 weak charge combination ( $2C_{2u} - C_{2d}$ ). In addition, the systematic uncertainty  
 67 goal was less than 3%. For this experiment, the expected asymmetries were 91 and  
 68 160 ppm respectively at the two  $Q^2$  values. To achieve the required precision, an  
 69 event rate capability of up to 500 kHz was needed.

70 The main challenge of deep inelastic scattering experiments is the separation of  
 71 scattered electrons from the pion background in the spectrometer and detector sys-  
 72 tem. The neutral pions would decay into  $e^+e^-$  pairs, from which the electrons pro-  
 73 duced cannot be rejected by detectors and their effect on the measured asymmetry  
 74 was analyzed in Ref. [3]. Charged pions are produced primarily from nucleon res-  
 75 onance decays and could carry a parity violation asymmetry corresponding to the  
 76  $Q^2$  at which the resonances are produced, typically a fraction of the asymmetry of  
 77 electrons with the same scattered momentum. Assuming that a fraction  $f_{\pi/e}$  of the  
 78 detected events are  $\pi^-$  and  $1 - f_{\pi/e}$  are electrons, the measured asymmetry is

$$A_m = f_{\pi/e}A_\pi + (1 - f_{\pi/e})A_e, \quad (2)$$

79 where  $A_e$  is the desired electron scattering asymmetry and  $A_\pi$  is the asymmetry of  
 80 the pion background. To extract  $A_e$  to a high precision, one needs either to mini-  
 81 mize the pion contamination  $f_{\pi/e}$  to a negligible level, or to correct the measured  
 82 asymmetry for the asymmetry of pions, which itself needs to be measured precisely.  
 83 For the PVDIS experiment, the goal was to control  $f_{\pi/e}$  to the  $10^{-4}$  level provided  
 84 that the pion asymmetries did not exceed those of electrons.

85 The experiment used a 100  $\mu$ A electron beam with a polarization of approximately  
 86 90% and a 20-cm long liquid deuterium target. The two High Resolution Spec-  
 87 trometers (HRS) [5] were used to detect scattered events. While the standard HRS  
 88 detector package and data acquisition (DAQ) system routinely provide a  $10^4$  pion  
 89 rejection with approximately 99% electron efficiency, they are based on full record-  
 90 ing of the detector signals and are limited to event rates up to 4 kHz [5]. This is not  
 91 sufficient for the high rates expected for the experiment. (The HRS DAQ will be  
 92 referred to as “standard DAQ” hereafter.)

93 Recent parity violation electron scattering experiments, such as HAPPEX [7,8,9,10,11],  
 94 and PREX [12] at JLab, focused on elastic scattering from nuclear or nucleon tar-  
 95 gets that are typically not contaminated by inelastic backgrounds. Signals from the  
 96 detectors can be integrated and a helicity dependence in the integrated signal can  
 97 be used to extract the physics asymmetry. An integrating DAQ was also used in  
 98 the preceding PVDIS measurement at SLAC [13,14] in which approximately 2%  
 99 of the integrated signal was attributed to pions. The SAMPLE experiment [6] at  
 100 MIT-Bates focused also on elastic scattering but the inelastic contamination was  
 101 more challenging to reject, and an air Cherenkov counter was used to select only  
 102 elastic scattering events. In the Mainz PVA4 experiment [15,16,17], particles were

103 detected in a total absorption calorimeter and the integrated energy spectrum was  
104 recorded. Charged pions and other background were separated from electrons in  
105 the offline analysis of the energy spectrum, and the pion rejection was on the order  
106 of 100:1 based on the characteristics of the calorimeter.

107 High performance particle identification can usually be realized in a counting-based  
108 DAQ where each event is evaluated individually. In the G0 experiment [18,19,20,21,22]  
109 at JLab, a superconducting spectrometer with a  $2\pi$  azimuthal angle coverage was  
110 used to detect elastically scattered protons at the forward angle and elastic elec-  
111 trons at the backward angle. At the forward angle, protons were identified using  
112 time-of-flight. At the backward angle, pions were rejected from electrons using an  
113 aerogel Cherenkov counter, and a pion rejection factor of 125 : 1 or better was  
114 reported [22]. The deadtime correction of the counting system was on the order of  
115 a few percent [21,22].

116 While the PVDIS experiment could fully utilize existing spectrometers and detec-  
117 tors at JLab, examination of all existing techniques for PV measurements made it  
118 clear that a custom electronics and DAQ were needed to keep the systematic uncer-  
119 tainties due to data collection to below 1%. In this paper we describe a scaler-based,  
120 cost effective counting DAQ which limited the pion contamination of the data sam-  
121 ple to a negligible level of  $f_{\pi/e} \approx 10^{-4}$ . Basic information on the detector package  
122 and the DAQ setup will be presented first and followed by the analysis of electron  
123 detection efficiency, pion rejection and contamination, corrections due to counting  
124 deadtime, and the statistical quality of the asymmetry measurement.

## 125 **2 Detector and DAQ Overview**

126 The design goal of the DAQ is to record data up to 1 MHz with hardware-based  
127 PID and well measured and understood deadtime effects. The following detectors  
128 in the HRS [5] were used to characterize scattered particles: Two scintillator planes  
129 provided the main trigger, while a  $\text{CO}_2$  gas Cherenkov detector and a double-layer  
130 segmented lead-glass detector provided particle identification information. The ver-  
131 tical drift chambers (as the tracking detector) were used during calibration runs but  
132 were turned off during production data taking because they were not expected to  
133 endure the high event rates.

134 For the gas Cherenkov and the lead-glass detector, a full recording of their output  
135 ADC data was not feasible at the expected high rate. Instead their signals were  
136 passed through discriminators and logic units to form preliminary electron and pion  
137 triggers. Particle identification was fulfilled by the use of discriminators for both  
138 the lead-glass and the Cherenkov detectors and proper settings of their thresholds.  
139 These preliminary triggers were then combined with the scintillator triggers to form  
140 the final electron and pion triggers, which were sent to scalers to record the event

141 counts and used offline to form asymmetries  $A = (n_R - n_L)/(n_R + n_L)$ , where  $n_{R(L)}$   
142 is the integrated rate of the triggers normalized to the integrated beam charge for  
143 the right( $R$ ) and left( $L$ ) handed spin (helicity) states of the incident electron beam.  
144 The scalers that counted triggers and the beam charge were integrated over the  
145 helicity period, which was flipped pseudo-randomly at 30 Hz per the experimental  
146 technique used by the HAPPEX experiments [11].

147 For the HRS the two layers of the lead-glass detector are called “preshower” and  
148 “shower” detectors, respectively. The preshower in the Right HRS (the spectrome-  
149 ter located to the right side of the beamline when viewed along the beam direction)  
150 has 48 blocks arranged in a  $2 \times 24$  array, with the longest dimension of the blocks  
151 aligned perpendicular to the particle trajectory. For the two blocks in each row, only  
152 the ends facing outward are read out by photo-multiplier tubes (PMTs), while the  
153 other ends of the two blocks are facing each other and not read out. Therefore, the  
154 preshower detector has 48 output channels. All preshower blocks were individually  
155 wrapped to prevent light leak. The shower detector in the Right HRS had 75 blocks  
156 arranged in a  $5 \times 15$  array with the longest dimension of the blocks aligned along  
157 the trajectory of scattered particles. PMTs were attached to each block of the Right  
158 shower detector on one end only, giving 75 output channels. The preshower and the  
159 shower detectors in the Left HRS are similar to the preshower detector on the Right  
160 HRS except that for each detector there are 34 blocks arranged in a  $2 \times 17$  array.

161 Because the lead-glass detectors in the Left and Right HRS are different, design of  
162 the lead-glass-based triggers of the DAQ is also different, as shown in Fig. 1. As a  
163 compromise between the amount of electronics needed and the rate in the front end  
164 logic modules, the lead-glass blocks in both the preshower and the shower detectors  
165 were divided into 6 (8) groups for the Left (Right) HRS, with each group consisting  
166 8 blocks. On the Right HRS only 60 of the 75 shower blocks were used while the 15  
167 blocks on the edge were not read out. The reduction of the HRS acceptance due to  
168 not using these side blocks was negligible. Signals from the 8 blocks in each group  
169 were added using a custom-made analog summing unit called the “SUM8 module”,  
170 then passed to discriminators. The geometry and the position of each preshower  
171 group were carefully chosen to match those of the corresponding shower group  
172 to maximize electron detection efficiency. On the Left HRS, adjacent groups in  
173 both preshower and shower had overlapping blocks, while for the Right HRS only  
174 preshower blocks were overlapping. To allow overlap between adjacent groups,  
175 signals from preshower blocks on the Right HRS and from both preshower and  
176 shower blocks on the Left HRS were split into two identical copies using passive  
177 splitters.

178 A schematic diagram of the DAQ electronics for the Right HRS is shown in Fig. 2.  
179 Preliminary electron and pion triggers were formed by passing shower (SS) and  
180 preshower (PS) signals and their sums, called total shower (TS) signals, through  
181 discriminators with different thresholds. For electron triggers, logical ANDs of  
182 the PS discriminator and the TS discriminator outputs were used. For pions, low

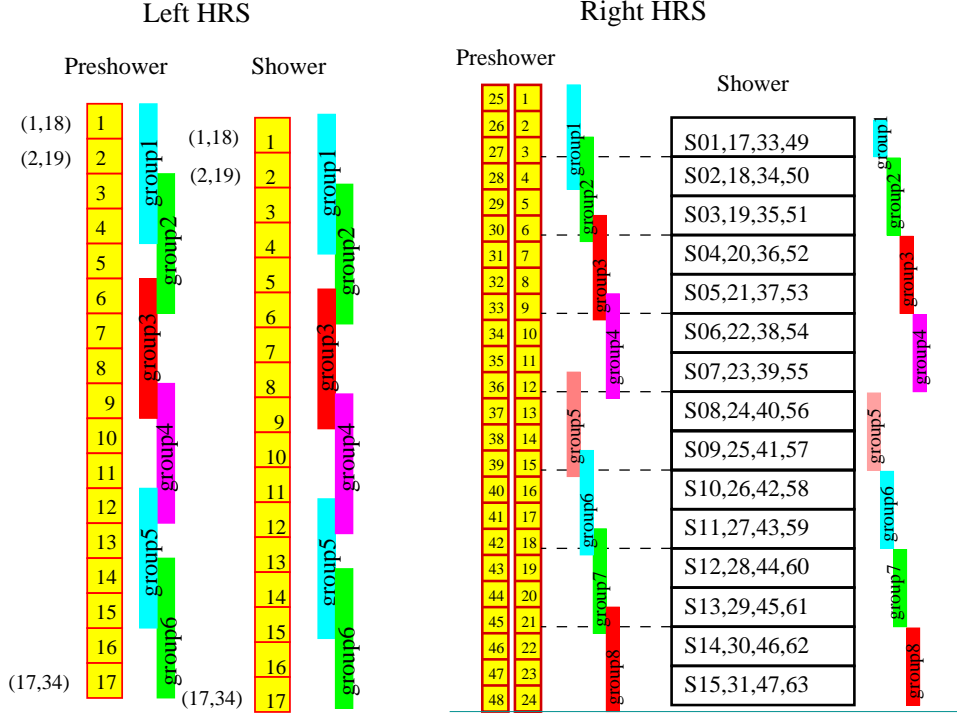


Fig. 1. [Color online] Grouping scheme (side-view) for the double-layer lead-glass detectors for the Left and the Right HRS. Scattered particles enter the detector from the left. The colored vertical bars represent the range of each group.

183 threshold discriminators on the TS signal alone were sent to logical OR modules  
 184 to produce preliminary triggers. Additional background rejection was provided by  
 185 the “GATE” circuit, which combined signals from the gas Cherenkov (GC) and the  
 186 “T1” signal [5] from the scintillators (SC). Each valid coincidence between GC and  
 187 T1 would produce a 150-ns wide electron GATE signal that allowed an output to be  
 188 formed by the logical AND modules from the preliminary electron triggers. Each  
 189 valid T1 signal without the GC signal would produce a 150-ns wide pion GATE  
 190 signal that allowed an output to be formed by the logical OR modules from the  
 191 preliminary pion triggers. The outputs of the logical AND and OR modules are  
 192 called group electron and pion triggers, respectively. All six (eight) group electron  
 193 or pion triggers were then Ored together to form the global electron or pion trigger  
 194 for the Left (Right) HRS. All group and the final electron and pion triggers were  
 195 counted using scalers. Because pions do not produce large enough lead-glass sig-  
 196 nals to trigger the high threshold TS discriminators for the electron triggers, pions  
 197 do not introduce extra counting deadtime for the electron triggers. However, the  
 198 150-ns width of the electron GATE signal would cause pion contamination in the  
 199 electron trigger. This effect will be presented in section 3.

200 In order to monitor the counting deadtime of the DAQ, two identical paths of elec-  
 201 tronics were constructed. The only difference between the two paths is in the PS  
 202 and the TS discriminator output widths, set at 30 ns and 100 ns for the “narrow” and  
 203 the “wide” paths, respectively. The scalers are rated for 250 MHz (4 ns deadtime)

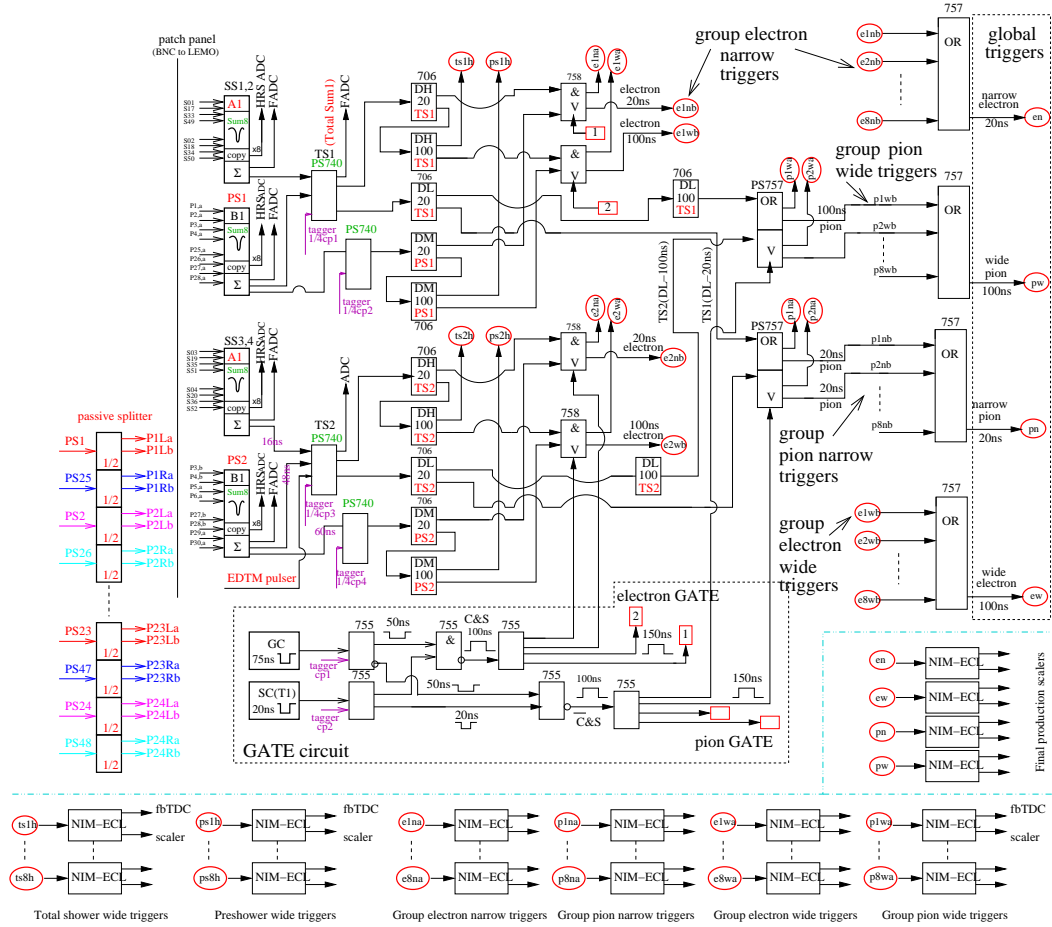


Fig. 2. [Color online] Electronics diagram for the Right HRS DAQ used by the PVDIS experiment. The Sum8's, discriminators and logic modules for two groups are shown, as well as the location of tagger signal inputs, setup of the GATE circuit using scintillator (SC) and gas Cherenkov (GC) signals, the logic units for combining triggers from all eight groups into final triggers, the counting scalers, and the monitoring fastbus TDCs. Electronics for the Left HRS are similar except for the grouping scheme.

204 and therefore do not add to the deadtime. In addition, the output width of all logic  
 205 modules was set to 15 ns, so the deadtime of the DAQ for each group is dominated  
 206 by the deadtime of the discriminators. Detailed analysis of the DAQ deadtime will  
 207 be presented in section 4.

208 The SUM8 modules used for summing all lead-glass signals also served as fan-out  
 209 modules, providing exact copies of the input PMT signals. These copies were sent  
 210 to the standard HRS DAQ for calibration. During the experiment, data were col-  
 211 lected at low rates using reduced beam currents with both DAQs functioning, such  
 212 that a direct comparison of the two DAQs could be made. Vertical drift chambers  
 213 were used during these low rate DAQ studies. Outputs from all discriminators, sig-  
 214 nals from the scintillator and the gas Cherenkov, and all electron and pion group  
 215 and global triggers were sent to Fastbus TDCs (fbTDC) and were recorded in the  
 216 standard DAQ. Data from these fbTDCs were used to align the amplitude spectrum

217 and timing of all signals. They also allowed the study of the Cherenkov and the  
218 lead-glass detector performance for the new DAQ.

219 Full sampling of partial analog signals was done using Flash-ADCs (FADCs) at  
220 low rates intermittently during the experiment. For one group on the Left and one  
221 group on the Right HRS, the preshower and the shower SUM8 outputs, the inter-  
222 mediate logical signals of the DAQ, and the output electron and pion triggers were  
223 recorded. These FADC data provided a study of pileup effects to confirm the dead-  
224 time simulation and to provide the input parameters for the simulation, specifically  
225 the rise and fall times of the signals and their widths.

### 226 3 DAQ PID Performance

227 The PID performance of the DAQ system was studied with calibration runs taken at  
228 low beam currents using fbTDC signals along with ADC data of all detector signals  
229 recorded by the standard DAQ. Events that triggered the DAQ would appear as a  
230 timing peak in the corresponding fbTDC spectrum of the standard DAQ, and a cut  
231 on this peak can be used to select those events. Figure 3 shows the preshower vs.  
232 shower signals for group 2 on the Left HRS. A comparison between no fbTDC  
233 cut and with cut on the fbTDC signal of the electron wide trigger from this group  
clearly shows the hardware PID cuts.

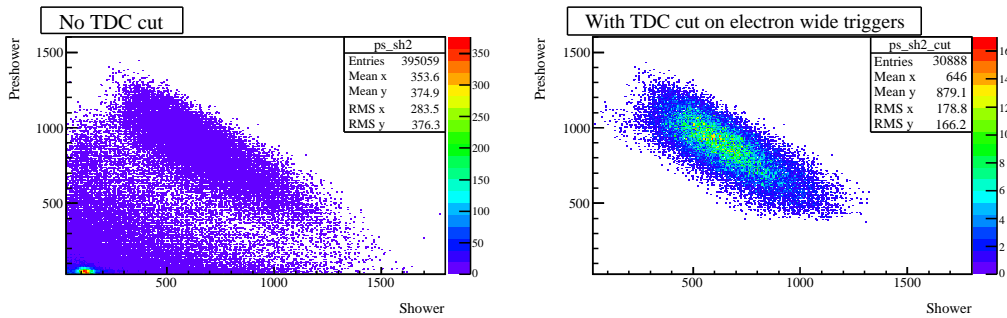


Fig. 3. [Color online] Preshower vs. Shower ADC data (sum of 8 blocks each) for group 2 on the Left HRS, without the fbTDC cut (left panel) and with cut on the group 2 electron wide trigger fbTDC signal (right panel). This clearly shows the thresholds of the preshower and the total shower signals, indicating that the DAQ is selecting the correct events as electrons.

234

235 Electron efficiency and pion rejection factors of the lead-glass detector on the Left  
236 HRS during a one-hour run are shown in Fig. 4 as functions of the location of the  
237 hit of the particle in the preshower detector. PID performance on the Right HRS is  
238 similar. Electron efficiency from wide groups is slightly higher than from narrow  
239 groups because there is less event loss due to timing misalignment when taking  
240 the coincidence between the preshower and the total shower discriminator outputs.

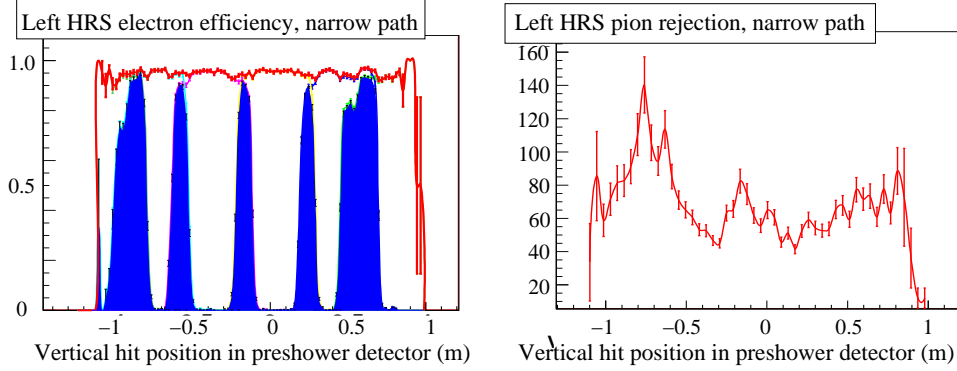


Fig. 4. [Color online] Electron detection efficiency (left) and pion rejection factor (right) vs. vertical (dispersive) hit position of the particle in the preshower detector for the narrow electron triggers in the Left HRS. An 8-minute run with a reduced beam current of  $2 \mu\text{A}$  at the  $Q^2 = 1.9 \text{ (GeV}/c)^2$  setting was used in this evaluation. For electron efficiencies, the total efficiency is shown by the red curve, while blue shaded area indicates events that were recorded by two adjacent groups. The average electron efficiency achieved by the lead glass detector alone for this run is  $(94.60 \pm 0.11)\%$  and the average pion rejection factor is  $(76.2 \pm 1.5) : 1$  (the error bars are statistical only). PID performance for the wide path and the Right HRS are similar.

241 Variations in the electron efficiency across the spectrometer acceptance effectively  
 242 influence the  $Q^2$  of the measurement. For this reason, low-rate calibration data  
 243 were taken daily during the experiment to monitor the DAQ PID performance, and  
 244 corrections were applied to the asymmetry data.

245 The gas Cherenkov detector signals were read out by 10 PMTs on both the Left and  
 246 the Right HRS. Signals from all 10 PMTs were summed in an analog-sum module  
 247 and sent to a discriminator. The discriminator output was sent to the DAQ (as shown  
 248 in Fig. 2) as well as to fbTDCs. Figure 5 shows the Cherenkov ADC sum with and  
 249 without the fbTDC cut, which clearly shows the capability of rejecting pions.

250 As described in the Introduction, pion contamination in the electron trigger would  
 251 affect the measured electron asymmetry as  $A_m = (1 - f_{\pi/e})A_e + f_{\pi/e}A_\pi$  where  $A_m$   
 252 and  $A_e$  are the measured and the true electron asymmetries, respectively, and  $A_\pi$   
 253 is the parity violation asymmetry of pion production. The pion contamination in the  
 254 electron trigger,  $f_{\pi/e}$ , comes from two effects: There is a small possibility that a  
 255 pion could trigger both the lead-glass and the gas Cherenkov detectors, causing a  
 256 false electron trigger output. This possibility is determined by the direct combina-  
 257 tion of the pion rejection factors of the two detectors and is below  $10^{-4}$ . A larger  
 258 effect comes from the width of the electron GATE signal: Since each coincidence  
 259 between the gas Cherenkov and the scintillator signals would open the electron  
 260 counting GATE by 150 ns, while the DAQ deadtime of the lead-glass detector is  
 261 less than this value, pions that arrived after the DAQ deadtime but before the clos-  
 262 ing of the electron GATE signal would cause a false electron trigger. The sum of  
 263 the two effects can be written as

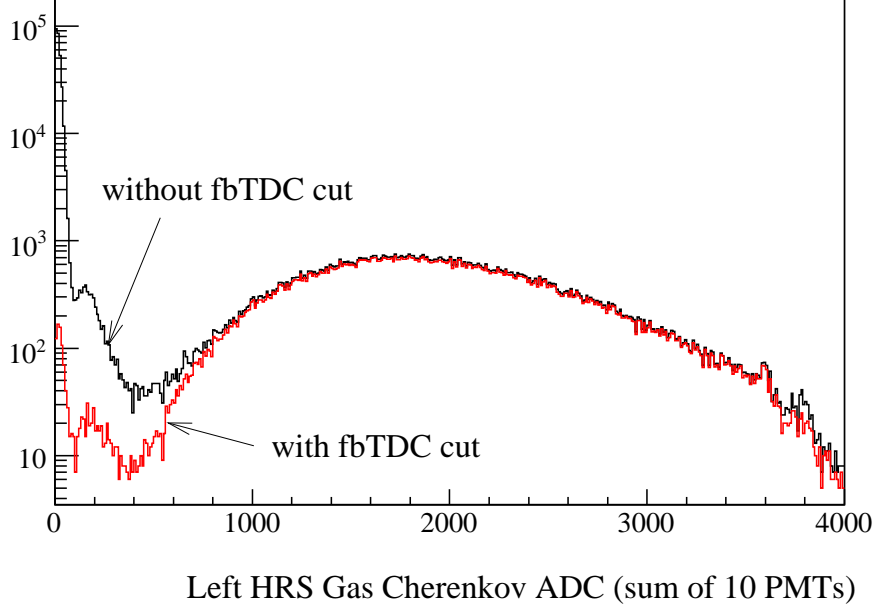


Fig. 5. [Color online] Gas Cherenkov ADC data (sum of 10 PMTs) for the Left HRS during a one-hour run at  $Q^2 = 1.9 \text{ (GeV}/c)^2$ , with a fbTDC cut on the Cherenkov discriminator output (red) and without (black). The beam current during this run was about  $100 \mu\text{A}$ , the incident electron rate on the detector was about  $23 \text{ kHz}$  with a pion to electron rate ratio of approximately 3.5. The discriminator clearly selected electrons while rejecting pions.

$$f_{\pi/e,n(w)} = \frac{R_{\pi}\eta_{\pi}^{GC}\eta_{\pi}^{LG}}{R_e\eta_e^{GC}\eta_e^{LG}} + \frac{R_{\pi}\eta^{LG} \left\{ R_e\eta_e^{GC} \left[ 150 \text{ ns} - \tau_{n(w)} \right] \right\}}{R_e\eta_e^{GC}\eta_e^{LG}}$$

264 where  $R_e$  and  $R_{\pi}$  are the input electron and the pion rates, respectively;  $\eta_e^{LG(GC)}$   
 265 is the electron detection efficiency of the lead-glass (gas Cherenkov) detectors, and  
 266  $\eta_{\pi}^{LG(GC)}$  is the pion detection efficiency, i.e., the inverse of the rejection factor, of  
 267 the lead-glass (gas Cherenkov) detector. The DAQ group deadtime of the lead-glass  
 268 detector for the narrow (wide) path,  $\tau_{n(w)}$ , is approximately 60 ns (100-110 ns) and  
 269 the analysis obtaining these results will be presented in the next section. The term  
 270  $R_e\eta_e^{GC} \left[ 150 \text{ ns} - \tau_{n(w)} \right]$  gives the probability of a pion's arriving within a valid  
 271 electron GATE signal and thus such a pion can not be rejected by the lead-glass  
 272 detectors.

273 The electron detection efficiency and pion rejection factor averaged throughout the  
 274 data production period are shown in table 1 for different kinematics and for the Left  
 275 and the Right HRS separately. Also shown are the  $\pi/e$  rate ratio obtained from the  
 276 data and the resulting pion contamination  $f_{\pi/e}$  evaluated separately for the narrow  
 277 and the wide paths.

278 As shown in table 1, the overall pion contamination was on the order of  $2 \times 10^{-4}$   
 279 or lower. Because pions are produced from nucleon resonance decays, the parity

Table 1

Average electron detection efficiency and pion rejection factor achieved through the lead glass (LG) and the gas Cherenkov (GC) detectors, respectively, and the combined performance. The error bars of the efficiencies and the rejection factors are statistical only. The error bars for  $f_{\pi/e}$ ,  $\Delta f_{\pi/e,n(w)}$ , are shown separately for statistical uncertainties, systematic uncertainties due to our understanding of the rates, detector efficiencies and deadtimes, and day-to-day variations in the measured detector efficiencies.

Kinematics and Spectrometer combinations			
	$Q^2 = 1.1 \text{ (GeV}/c)^2$	$Q^2 = 1.9 \text{ (GeV}/c)^2$	
HRS	Left	Left	Right
Electron detection efficiency $\eta_e$			
GC	$(99.14 \pm 0.02)\%$	$(99.03 \pm 0.03)\%$	$(98.19 \pm 0.06)\%$
LG, narrow	$(91.93 \pm 0.04)\%$	$(94.50 \pm 0.06)\%$	$(94.36 \pm 0.04)\%$
LG, wide	$(92.88 \pm 0.04)\%$	$(95.79 \pm 0.06)\%$	$(95.23 \pm 0.04)\%$
combined, narrow	$(91.14 \pm 0.04)\%$	$(93.58 \pm 0.06)\%$	$(92.65 \pm 0.07)\%$
combined, wide	$(92.08 \pm 0.04)\%$	$(94.86 \pm 0.06)\%$	$(93.51 \pm 0.07)\%$
Pion rejection $1/\eta_\pi$			
GC	$(158.6 \pm 3.5) : 1$	$(301.2 \pm 5.2) : 1$	$(414.3 \pm 6.2) : 1$
LG, narrow	$(101.5 \pm 1.6) : 1$	$(78.9 \pm 0.9) : 1$	$(72.7 \pm 0.3) : 1$
LG, wide	$(103.9 \pm 1.7) : 1$	$(81.5 \pm 1.0) : 1$	$(74.3 \pm 0.3) : 1$
Pion contamination in the electron trigger $f_{\pi/e}$ , narrow path			
actual rate $R_\pi/R_e$	$\approx 0.5$	$\approx 3.3$	$\approx 3.3$
$f_{\pi/e,n}$	$1.07 \times 10^{-4}$	$1.97 \times 10^{-4}$	$1.30 \times 10^{-4}$
$\Delta f_{\pi/e,n}(\text{stat.})$	$\pm 1.8 \times 10^{-6}$	$\pm 2.9 \times 10^{-6}$	$\pm 0.9 \times 10^{-6}$
$\Delta f_{\pi/e,n}(\text{syst.})$	$\pm 2.41 \times 10^{-5}$	$\pm 1.79 \times 10^{-5}$	$\pm 1.03 \times 10^{-5}$
$\Delta f_{\pi/e,n}(\text{total})$	$\pm 2.42 \times 10^{-5}$	$\pm 1.81 \times 10^{-5}$	$\pm 1.04 \times 10^{-5}$
Pion contamination in the electron trigger $f_{\pi/e}$ , wide path			
$f_{\pi/e,w}$	$0.72 \times 10^{-4}$	$1.64 \times 10^{-4}$	$0.92 \times 10^{-4}$
$\Delta f_{\pi/e,w}(\text{stat.})$	$\pm 1.3 \times 10^{-6}$	$\pm 0.27 \times 10^{-6}$	$\pm 0.8 \times 10^{-6}$
$\Delta f_{\pi/e,w}(\text{syst.})$	$\pm 2.19 \times 10^{-5}$	$\pm 1.67 \times 10^{-5}$	$\pm 1.26 \times 10^{-5}$
$\Delta f_{\pi/e,w}(\text{total})$	$\pm 2.19 \times 10^{-5}$	$\pm 1.69 \times 10^{-5}$	$\pm 1.26 \times 10^{-5}$

280 violation asymmetry of pion production is expected to be no larger than that of  
 281 scattered electrons with the same momentum. This was confirmed by asymmetries  
 282 formed from pion triggers during this experiment. The uncertainty in the electron  
 283 asymmetry due to pion contamination is therefore on the order of  $2 \times 10^{-4}$  and is  
 284 negligible compared with the 3 – 4% statistical uncertainty.

To understand fully the effect of pion background on the measured electron asymmetry, it is important to extract asymmetries of the pion background to confirm that they are indeed smaller than the electron asymmetry. A complete PID analysis was carried out on the pion triggers of the DAQ where the electron contamination in the pion trigger  $f_{e/\pi}$  was evaluated in a similar method as  $f_{\pi/e}$  above, following

$$f_{e/\pi, n(w)} = \frac{R_e \xi_e^{GC} \xi_e^{LG}}{R_\pi \xi_\pi^{GC} \xi_\pi^{LG}} + \frac{R_e \xi_e^{LG} \left\{ R_\pi \xi_\pi^{GC} [150 \text{ ns} - \tau_{n(w)}] \right\}}{R_\pi \xi_\pi^{GC} \xi_\pi^{LG}}$$

285 where as before  $R_e$  and  $R_\pi$  are the electron and the pion rates incident on the de-  
 286 tectors, respectively; The detection efficiencies  $\xi$  are now defined for the pion trig-  
 287 gers of the DAQ:  $\xi_e^{LG(GC)}$  is the electron detection efficiency of the lead-glass (gas  
 288 Cherenkov) detectors, and  $\xi_\pi^{LG(GC)}$  is the pion detection efficiency of the lead-glass  
 289 (gas Cherenkov) detector in the pion triggers. Although the goal of the pion triggers  
 290 is to collect pions, only the gas Cherenkov played a role in rejecting electrons in  
 291 the pion trigger, and all electrons would form valid pion triggers in the lead-glass  
 292 counters. Therefore  $\xi_e^{LG} \approx 1$  and the electron contamination is high. Results for  
 293 electron contamination in the pion trigger are summarized in Table 2.

## 294 4 DAQ Deadtime

295 Deadtime is the amount of time after an event during which the system is unable  
 296 to record another event. Identifying the exact value of the deadtime is always a  
 297 challenge in counting experiments. By having a narrow and a wide path, we can  
 298 observe the trend in the deadtime: The wider path should have higher deadtime. By  
 299 matching the observed trend with our simulation we can benchmark and confirm  
 300 the result of our deadtime simulation. In addition, dividing lead-glass blocks into  
 301 groups greatly reduces the deadtime loss in each group compared with summing  
 302 all blocks together and forming only one final trigger.

303 To illustrate the importance of the deadtime, consider its effect on the asymmetry  $A$ .  
 304 For a simple system with only one contribution to the deadtime loss  $\delta$ , the observed  
 305 asymmetry  $A_O$  is related to the true asymmetry  $A$  according to  $A_O = (1 - \delta)A$ . In  
 306 this experiment  $\delta$  was expected to be on the order of (1-2)%. Since the statistical  
 307 accuracy of the asymmetry is (3-4)%, it was desirable to know  $\delta$  with a (10-20)%  
 308 relative accuracy so that it would become a negligible systematic error. The DAQ  
 309 used in this experiment, however, was more complex and had three contributions

Table 2

Average pion detection efficiency and electron rejection factor achieved through the lead glass (LG) and the gas Cherenkov (GC) detectors, respectively, and the combined performance. The error bars of the efficiencies and the rejection factors are statistical only. The error bars for  $f_{e/\pi}$ ,  $\Delta f_{e/\pi,n(w)}$ , are shown separately for statistical uncertainties, systematic uncertainties, and day-to-day variations in the measured detector efficiencies.

Kinematics and Spectrometer Combinations			
	$Q^2 = 1.1 \text{ (GeV}/c)^2$	$Q^2 = 1.9 \text{ (GeV}/c)^2$	
HRS	Left	Left	Right
Pion detection efficiency $\eta_\pi$			
GC	$(99.52 \pm 0.01)\%$	$(99.73 \pm 0.01)\%$	$(99.74 \pm 0.01)\%$
LG, narrow	$(21.67 \pm 0.01)\%$	$(79.72 \pm 0.02)\%$	$(15.61 \pm 0.01)\%$
LG, wide	$(21.67 \pm 0.01)\%$	$(79.71 \pm 0.02)\%$	$(15.60 \pm 0.01)\%$
combined, narrow	$(21.57 \pm 0.01)\%$	$(79.70 \pm 0.02)\%$	$(15.57 \pm 0.01)\%$
combined, wide	$(21.57 \pm 0.01)\%$	$(79.69 \pm 0.02)\%$	$(15.56 \pm 0.01)\%$
Electron rejection $1/\eta_e$			
GC	$(31.42 \pm 0.78) : 1$	$(89.44 \pm 2.48) : 1$	$(48.48 \pm 1.55) : 1$
LG, narrow	$(1.0468 \pm 0.0003) : 1$	$(1.0487 \pm 0.0005) : 1$	$(1.0271 \pm 0.0002) : 1$
LG, wide	$(1.0469 \pm 0.0003) : 1$	$(1.0499 \pm 0.0005) : 1$	$(1.0279 \pm 0.0002) : 1$
Electron contamination in pion triggers $f_{e/\pi}$ , narrow path			
actual rate $R_\pi/R_e$	$\approx 0.5$	$\approx 3.3$	$\approx 3.3$
$f_{e/\pi,n}$	0.2653	0.03309	0.01027
$\Delta f_{e/\pi,n}(\text{stat.})$	$\pm 0.00287$	$\pm 0.00060$	0.00020
$\Delta f_{e/\pi,n}(\text{syst.})$	$\pm 0.06019$	$\pm 0.00333$	0.00125
$\Delta f_{e/\pi,n}(\text{total})$	$\pm 0.06025$	$\pm 0.00338$	0.00127
Electron contamination in pion triggers $f_{e/\pi}$ , wide path			
$f_{e/\pi,w}$	0.2176	0.02808	0.00907
$\Delta f_{e/\pi,w}(\text{stat.})$	$\pm 0.00286$	$\pm 0.00060$	0.00020
$\Delta f_{e/\pi,w}(\text{syst.})$	$\pm 0.05726$	$\pm 0.00360$	0.00124
$\Delta f_{e/\pi,w}(\text{total})$	$\pm 0.05734$	$\pm 0.00365$	0.00125

310 to the deadtime as listed below:

- 311 (1) The “group” deadtime: deadtime due to discriminators and logical AND mod-  
312 ules used to form group triggers;
- 313 (2) The “GATE” deadtime: deadtime from the GATE circuit that used scintillators  
314 and gas Cherenkov signals to form the GATE signals, which controlled the  
315 AND (OR) module of each group to form group electron (pion) triggers.
- 316 (3) The “OR” deadtime: deadtime due to the logical OR module used to combine  
317 all group triggers into final global triggers.

318 The total deadtime is a combination of all three. In order to evaluate the DAQ  
319 deadtime, a full-scale trigger simulation is necessary. This trigger simulation will  
320 be described in the next section followed by results on the group, GATE, and OR  
321 deadtime as well as on the total deadtime correction that was applied to the asym-  
322 metry data.

#### 323 4.1 Trigger Simulation

324 The Hall A Trigger Simulation (HATS) was developed for the purpose of dead-  
325 time study for this experiment. The inputs to HATS include the analog signals for  
326 preshower, shower, scintillator and gas Cherenkov. The signal amplitudes were pro-  
327 vided by ADC data from low-current runs, and the signal rates were from high-  
328 current production runs. The rise and fall times for the preshower and shower  
329 SUM8 outputs play an important role in HATS. The signal shape is simulated by  
330 the function  $S(t) = Ate^{-t/\tau}$ , where  $A$  is related to the amplitude of the signal, and  
331 the time constant  $\tau$  was determined from FADC data, see Fig. 6.

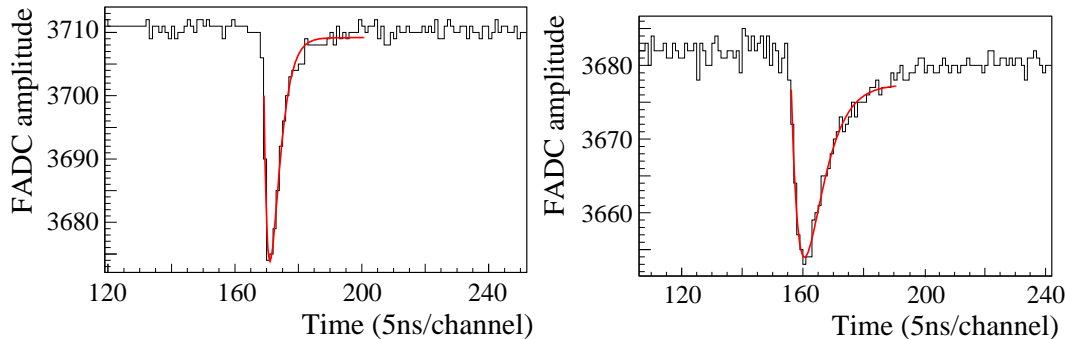


Fig. 6. [Color online] Calibration of time constants  $\tau$  for Preshower (left) and Shower (right) of the Right HRS. The FADC snapshot (black) is compared with the fit  $S(t) = Ate^{-t/\tau}$  (red). The time constant  $\tau$  was found to be approximately 11 ns for the Right HRS Preshower, and 21 – 22 ns for the Left HRS Preshower and Shower as well as for the Right HRS Shower.

332 With the recorded DAQ electronics and delay cables, HATS first rebuilds the DAQ  
333 system on the software level. At each nano-second, detector input signals are gen-

334 erated randomly according to the actual event rates and signal shape, and HATS  
 335 simulates output signals from all discriminators, AND, and OR modules. Figure 7  
 336 shows a fraction of the DAQ electronics and the simulated results for a very short  
 337 time period. By comparing output with input signals, HATS provides results on the  
 338 fractional loss due to deadtime for all group and global triggers with respect to the  
 339 input signal.

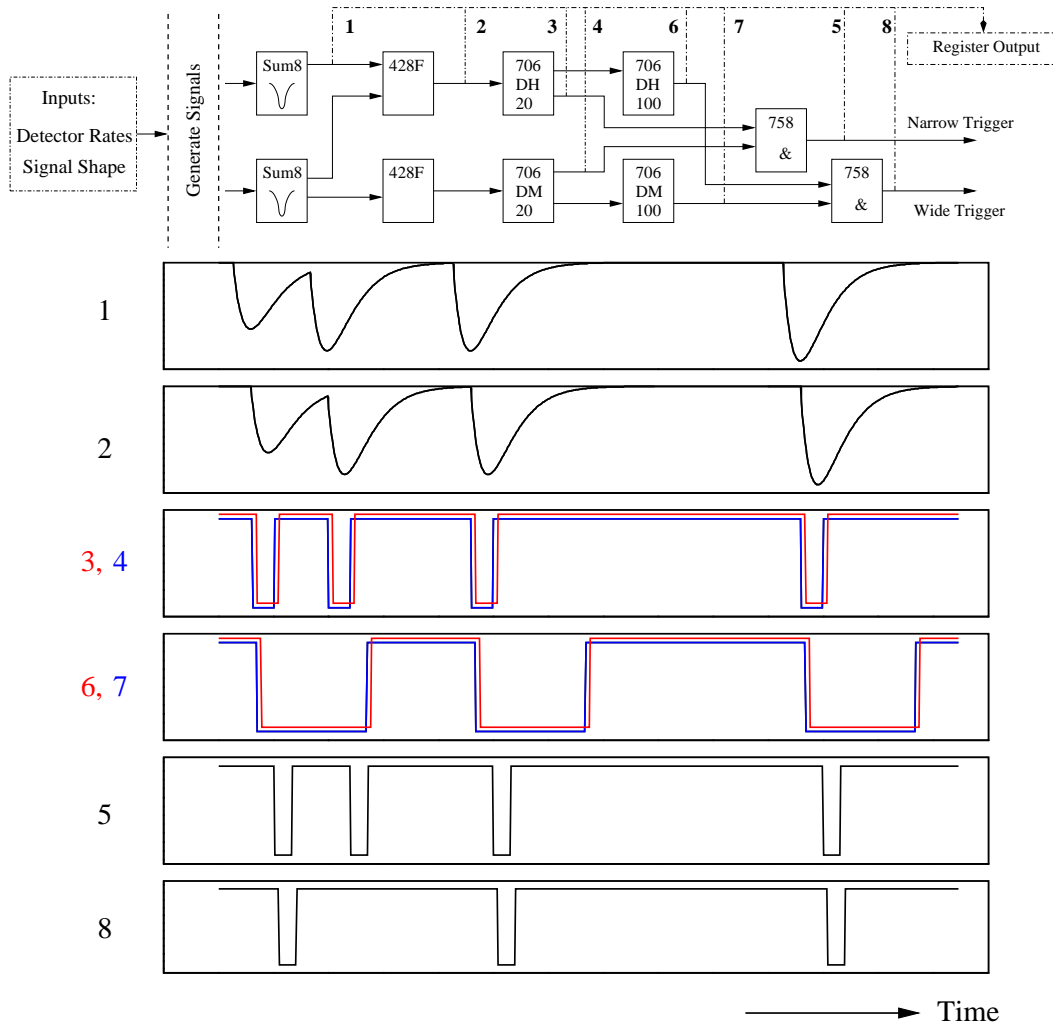


Fig. 7. [Color online] Top: A fraction of the group electron trigger. Each point corresponds to: 1 – Shower sum of the group; 2 – Total shower sum of the group; 3 – Total shower discriminator output (high threshold), narrow path; 4 – Preshower discriminator output (medium threshold), narrow path; 5 – group electron trigger, narrow path; 6 – Total shower discriminator output, wide path; 7 – Preshower discriminator output, wide path; 8 – group electron trigger, wide path. Bottom: Signals 1-8 as simulated by HATS. One can see that the second physical event is recorded by the narrow path group trigger (5) but not the wide path (8) due to deadtime loss.

340 4.2 Group Deadtime Measurement

341 In order to study the group deadtime, a high rate pulser signal (“tagger”) was mixed  
 342 with the Cherenkov and all preshower and total shower signals using analog sum-  
 343 ming modules, see Figs. 2 and 8. In the absence of all detector signals, a tagger  
 344 pulse produces without loss an electron trigger output and a “tagger-trigger coinci-  
 345 dence” pulse between this output and the “delayed tagger” – the tagger itself with  
 346 an appropriate delay to account for the DAQ response time. When high-rate detec-  
 347 tor signals are present, however, some of the tagger pulses would not be able to  
 348 trigger the DAQ due to deadtime. The deadtime loss in the electron trigger output  
 349 with respect to the tagger input has two components:

- 350 (1) The count loss  $R_o/R_i$ : When a detector PMT signal precedes the tagger signal  
 351 by a time interval  $\delta t$  shorter than the DAQ deadtime but longer than  $w + t_1$ ,  
 352 the tagger signal is lost and no coincidence output is formed. Here  $w$  is the  
 353 width of the electron trigger output and  $t_1$  is the time interval by which the  
 354 delayed tagger precedes the tagger’s own trigger output, see Fig. 8. During  
 355 the experiment  $w$  was set to 15 ns for all groups, and  $t_1$  was measured at the  
 356 end of the experiment and found to be between 20 and 40 ns for all narrow  
 357 and wide groups of the two HRSs.
- 358 (2) The pileup fraction  $p$ : When a PMT signal precedes the tagger signal by a time  
 359 interval  $\delta t$  shorter than  $w + t_1$ , there would be coincidence output between the  
 360 delayed tagger and the electron output triggered by the detector PMT signal.  
 361 If furthermore  $\delta t$  is less than the DAQ deadtime (which is possible for this  
 362 experiment since the deadtime is expected to be as long as 100 ns for the wide  
 363 path), the tagger itself is lost due to deadtime, and the tagger-trigger coinci-  
 364 dence is a false count and should be subtracted. In the case where  $\delta t$  is shorter  
 365 than  $w + t_1$  but longer than the DAQ deadtime (not possible for this experiment  
 366 but could happen in general), the tagger itself also triggers a tagger-trigger co-  
 367 incidence, but in this case, there are two tagger-trigger coincidence events.  
 368 Both are recorded by the fbTDC if working in the multi-hit mode, and one is  
 369 a false count and should be subtracted.

370 The pileup effect can be measured using the delay between the tagger-  
 371 trigger coincidence output and the input tagger. This is illustrated in Fig. 8  
 372 and the pileup effect contributes to both  $I_1$  and  $I_2$  regions of the fbTDC spec-  
 373 trum. Fractions of  $I_1$  and  $I_2$  relative to  $I_0$  are expected to be  $I_1/I_0 = Rt_1$  and  
 374  $I_2/I_0 = Rw$ , respectively, where  $R$  is the PMT signal rate. The pileup effect  
 375 was measured using fbTDC spectrum for electron narrow and wide triggers  
 376 for all groups. Data for  $I_{1,2}$  extracted from fbTDC agree very well with the  
 377 expected values.

The relative loss of tagger events due to DAQ deadtime is evaluated as

$$D = 1 - (1 - p)(R_o/R_i), \quad (3)$$

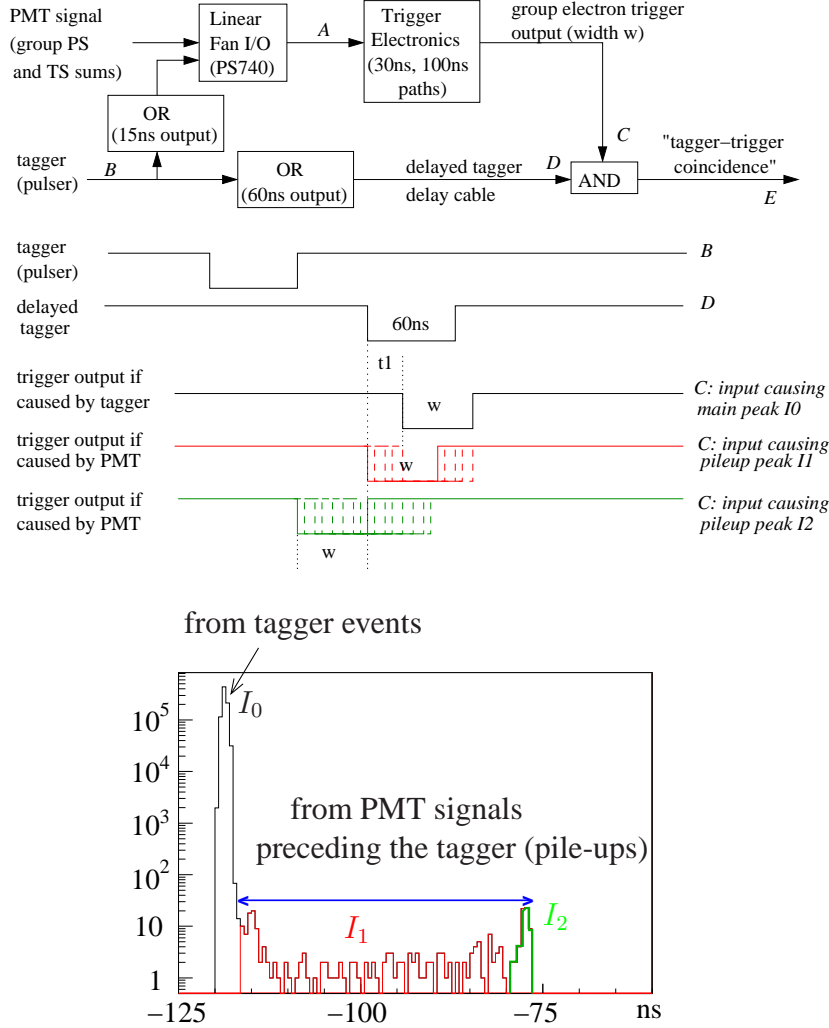


Fig. 8. [Color online] Top: schematic diagram for the tagger setup and signal timing sequence. The two logical OR units immediately following the tagger input “B” serve as width adjusters. Bottom: fbTDC spectrum for the relative timing between tagger-trigger coincidence and the input tagger, in 0.5-ns bins. The fbTDC module worked in a common stop and the multi-hit mode. Two different scenarios are shown: 1) Main peak  $I_0$ : when there is no PMT signal preceding the tagger, the tagger triggers the DAQ and forms a tagger-trigger coincidence. 2) Pileup events  $I_1$  and  $I_2$ : when there is a PMT signal preceding the tagger by a time interval shorter than  $w + t_1$ , the PMT signal triggers the DAQ and forms a tagger-trigger coincidence signal with the delayed tagger.

378 where  $R_i$  is the input tagger rate,  $R_o$  is the output tagger-trigger coincidence rate,  
 379 and  $p = (I_1 + I_2)/I_0$  is a correction factor for pileup effects as defined in Fig. 8.  
 380 Results for the deadtime loss  $D$  are shown in Figs. 9 and 10, for group 4 on the left  
 381 HRS and group 4 on the right HRS, respectively, and are compared with simula-  
 382 tion. Different beam currents between 20 and 100  $\mu\text{A}$  were used in this dedicated  
 383 deadtime measurement. In order to reduce the statistical fluctuation caused by the  
 384 limited number of trials in the simulation within a realistic computing time, simu-

385 lations were done at higher rates than the actual measurement.

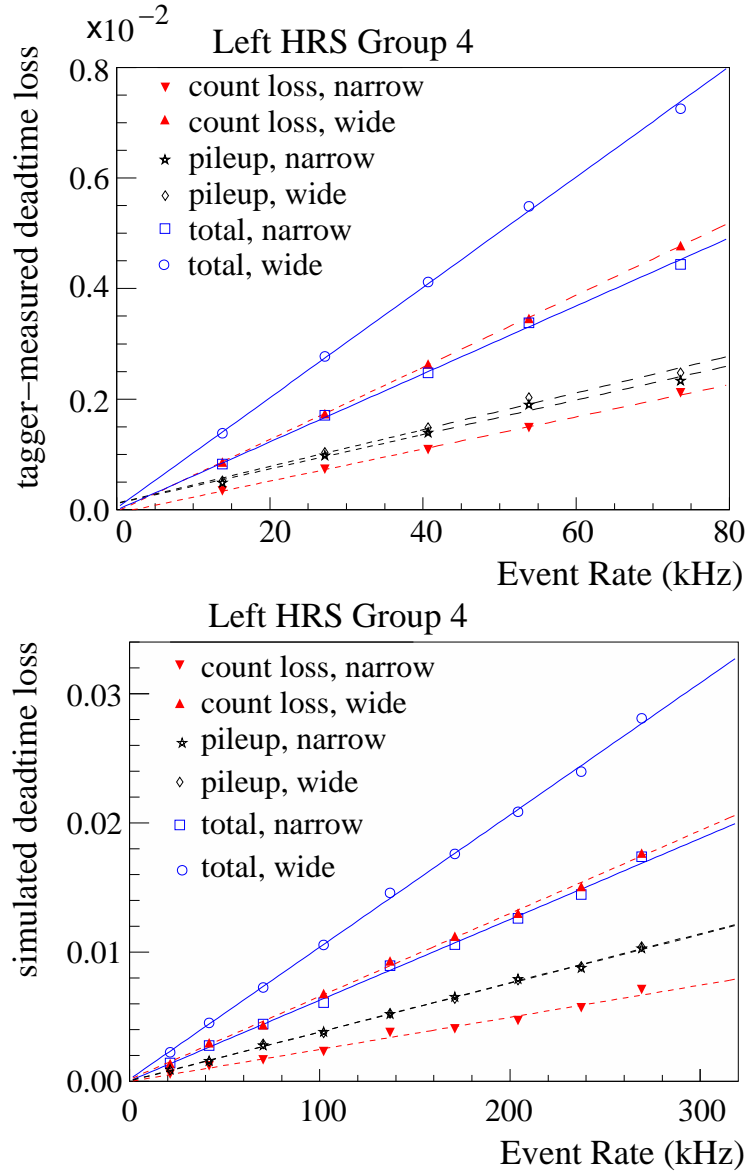


Fig. 9. [Color online] Deadtime loss in percent vs. event rate from the tagger method for group 4 on the Left HRS. Top: actual deadtime loss from tagger measurements; Bottom: simulated deadtime loss of the tagger. The tagger fractional count loss  $1 - R_o/R_i$  (red) and the pileup correction  $p$  (black) are combined to form the total group deadtime  $D$  (blue). These data were taken (or simulated) at a  $Q^2$  of  $1.1 \text{ (GeV}/c)^2$ . To minimize the statistical uncertainty while keeping the computing time reasonable, the simulation used higher event rates than the tagger measurement. The total group deadtime can be determined from the linear fit slope coefficients: tagger data narrow  $p_1 = (61.5 \pm 0.2) \times 10^{-9} \text{ s}$ , wide  $p_1 = (99.9 \pm 0.3) \times 10^{-9} \text{ s}$ , simulation narrow  $p_1 = (62.5 \pm 1.4) \times 10^{-9} \text{ s}$ , wide  $p_1 = (102 \pm 1.3) \times 10^{-9} \text{ s}$ . Group 4 is from the central blocks of the lead-glass detector and has the highest rate among all groups.

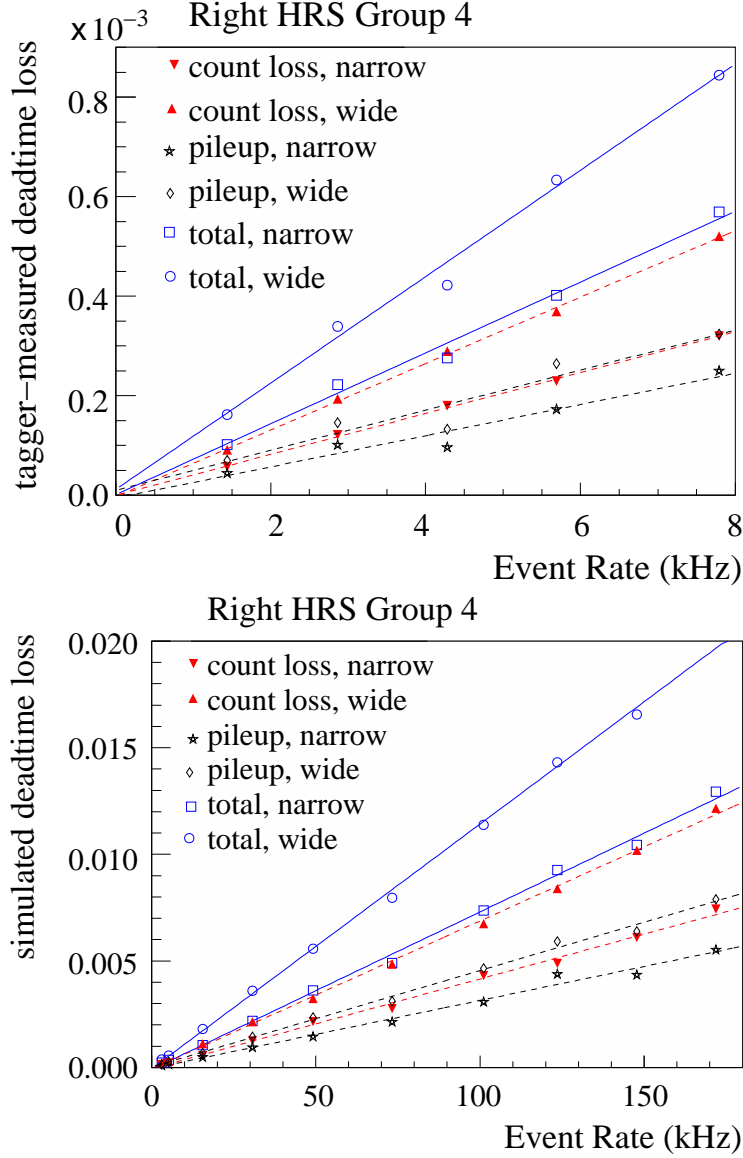


Fig. 10. [Color online] Deadtime loss in percent vs. group event rate from the tagger method for group 4 on the Right HRS. Top: tagger data; Bottom: simulation. These data were taken (or simulated) at a  $Q^2$  of 1.9 (GeV/c) $^2$ . The total group deadtime can be determined from the linear fit slope coefficient  $p_1$ : tagger data narrow  $p_1 = (71.1 \pm 0.9) \times 10^{-9}$  s, wide  $p_1 = (107 \pm 1.2) \times 10^{-9}$  s, simulation narrow  $p_1 = (73.9 \pm 1.5) \times 10^{-9}$  s, wide  $p_1 = (115 \pm 1.5) \times 10^{-9}$  s. Group 4 is from the central blocks of the lead-glass detector and has the highest rate among all groups. See Fig. 9 caption for details.

386 The slope of the tagger loss vs. event rate, as shown in Figs. 9 and 10, gives the  
 387 value of group deadtime in seconds. One can see that the deadtime for the wide path  
 388 is approximately 100 ns as expected. The deadtime for the narrow path, on the other  
 389 hand, is dominated by the input PMT signal width (typically 60-80 ns) instead of  
 390 the 30-ns discriminator width. The simulated group deadtime agrees with the data  
 391 at a 10% level or better, for both HRSs and for both wide and narrow paths.

392 4.3 Total Deadtime Evaluation

393 Although the deadtime loss of each group was measured using tagger signals, the  
 394 dominating term in the total deadtime is from the GATE electronics because the  
 395 trigger rate from scintillators and the gas Cherenkov is much higher than the indi-  
 396 vidual lead-glass group rates. The difference in total loss between narrow and wide  
 397 paths is thus smaller than that in their group deadtimes. Simulation for the GATE  
 398 deadtime was compared with FADC data and the agreement was found to be at a  
 399 20% level or better. After subtracting group and GATE deadtimes from the total  
 400 simulated deadtime, the remaining is attributed to the logical OR module. There is  
 401 no direct measurement of the logical OR deadtime, but the effect of the logical OR  
 402 module is quite straightforward and can be calculated analytically. The difference  
 403 between the simulation and the analytic results was used to estimate the uncertainty  
 404 of the OR deadtime.

405 The simulated deadtime loss of the global electron triggers and its decomposition  
 406 into group, GATE, and OR are shown in Table 3, along with the total deadtime  
 407 correction at a beam current of  $100 \mu\text{A}$ . The total deadtime loss not only increases  
 408 with higher electron rate  $R_e$ , but also with higher pion to electron ratio  $R_\pi/R_e$   
 409 which would cause larger GATE deadtime. The deadtime loss is also shown in  
 Fig. 11 as a function of the total event rate. Results shown in Table 3 provide a

Table 3

Simulated DAQ deadtime loss in percent for all kinematics and for both narrow (n) and wide (w) paths, along with the fractional contributions from group, GATE, and OR deadtimes. The fractional deadtime from OR is calculated as one minus those from group and GATE, and its uncertainty is estimated from the difference between simulation and the analytical results. The uncertainty of the total deadtime is the uncertainties from group, GATE and OR added in quadrature.

HRS, $Q^2$ (GeV/c) <sup>2</sup>	$R_e$ (kHz) $R_\pi/R_e$	Path	fractional contribution			Total deadtime loss at $100\mu\text{A}$
			Group	GATE	OR	
Left, 1.1	$\approx 210$	n	$(20.6 \pm 2.1)\%$	$(51.3 \pm 4.5)\%$	$(28.1 \pm 4.7)\%$	$(1.45 \pm 0.10)\%$
	$\approx 0.5$	w	$(29.5 \pm 2.4)\%$	$(45.3 \pm 4.0)\%$	$(25.3 \pm 4.6)\%$	$(1.64 \pm 0.11)\%$
Left, 1.9	$\approx 18$	n	$(5.42 \pm 0.8)\%$	$(81.1 \pm 7.1)\%$	$(13.5 \pm 7.0)\%$	$(0.50 \pm 0.05)\%$
	$\approx 3.3$	w	$(8.39 \pm 0.4)\%$	$(77.3 \pm 6.8)\%$	$(14.3 \pm 8.0)\%$	$(0.52 \pm 0.06)\%$
Right, 1.9	$\approx 18$	n	$(2.9 \pm 0.2)\%$	$(80.6 \pm 18.5)\%$	$(16.5 \pm 12.7)\%$	$(0.89 \pm 0.20)\%$
	$\approx 3.3$	w	$(4.3 \pm 0.4)\%$	$(76.6 \pm 17.5)\%$	$(19.1 \pm 15.5)\%$	$(0.93 \pm 0.22)\%$

410 direct correction to the measured asymmetry, and the uncertainties are small com-  
 411 pared with other dominant systematic uncertainties such as the beam polarization  
 412 measurement. In practice, the deadtime correction is applied to data on a run-by-  
 413 run basis with the deadtime of each run calculated using the actual beam current  
 414

415 during the run and the linear fitting results from Fig. 11.

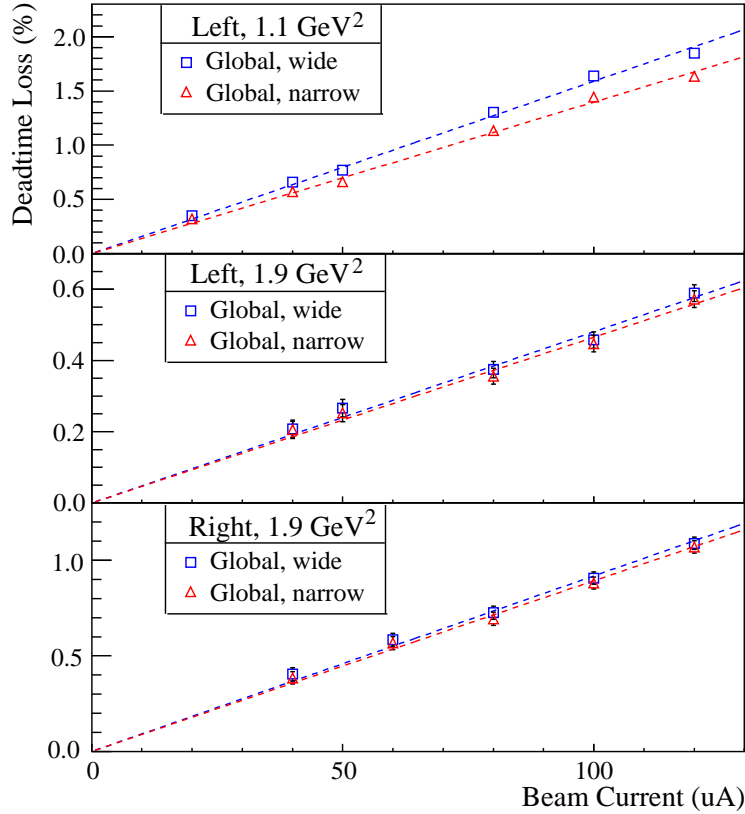


Fig. 11. [Color online] Simulated deadtime loss of the global electron trigger for the Left HRS at  $Q^2 = 1.1$  ( $\text{GeV}/c$ )<sup>2</sup> (top), the Left HRS at  $Q^2 = 1.9$  ( $\text{GeV}/c$ )<sup>2</sup> (middle), and the Right HRS at  $Q^2 = 1.9$  ( $\text{GeV}/c$ )<sup>2</sup> (bottom). The error bars shown are due to statistical uncertainty of the simulation. See Table 3 for final uncertainty evaluation.

#### 416 4.4 Asymmetry Measurement

417 The physics asymmetries sought for in this experiment were expected to be 91 and  
 418 160 ppm, for  $Q^2 = 1.1$  and  $1.9$  ( $\text{GeV}/c$ )<sup>2</sup>, respectively. The measured asymmetries  
 419 were about 90% of these values due to beam polarization. To understand the sys-  
 420 tematics of the asymmetry measurement, a half-wave plate (HWP) was inserted in  
 421 the beamline to flip the laser helicity in the polarized source during half of the data  
 422 taking period. The measured asymmetries flipped sign for each beam HWP change  
 423 and the magnitude of the asymmetry remained consistent within statistical error  
 424 bars.

425 The asymmetries can be formed from event counts of each beam helicity pair, with  
 426 33-ms of helicity right and 33-ms of helicity left beam, normalized by the beam  
 427 charge. Figure 12 shows the pull distribution of these pair-wise asymmetries with  
 428 the “pull” defined as

$$p_i \equiv (A_i - \langle A \rangle) / \delta A_i, \quad (4)$$

429 where  $A_i$  is the asymmetry extracted from the  $i$ -th beam helicity pair with the HWP  
 430 states already corrected and  $\delta A_i = 1/\sqrt{N_i^R + N_i^L}$  its statistical uncertainty with  
 431  $N_i^{R(L)}$  the event count from the right (left) helicity pulse of the pair, and  $\langle A \rangle$  is the  
 432 asymmetry averaged over all beam pairs. One can see that the asymmetry spectrum  
 433 agrees to five orders of magnitude with the Gaussian distribution, as expected from  
 434 purely statistical fluctuations.

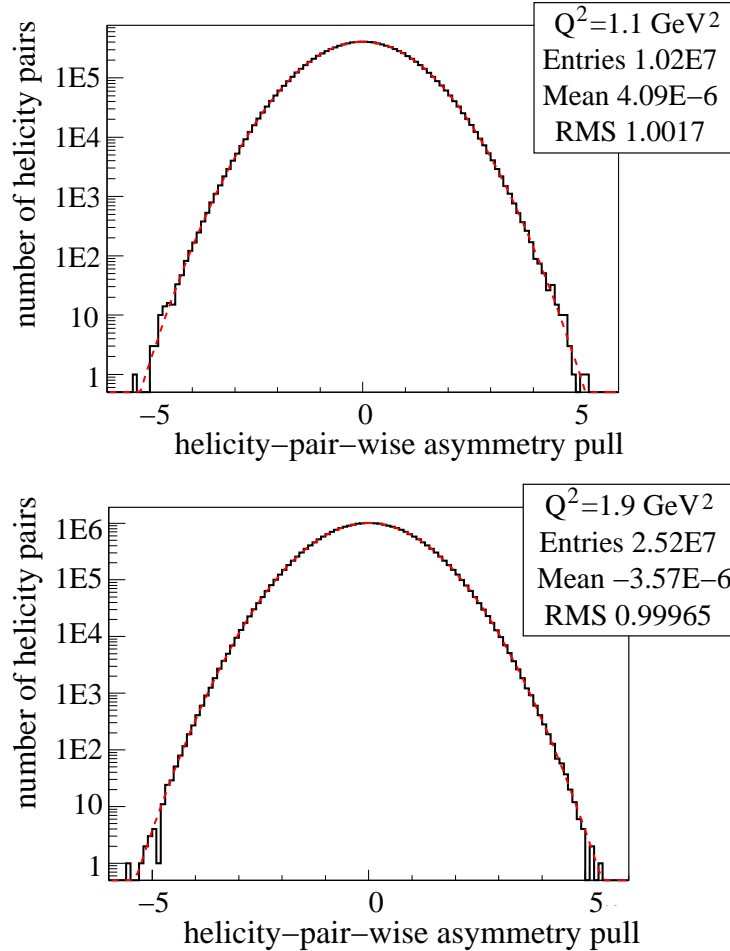


Fig. 12. [Color online] Pull distribution [Eq.(4)] for the global electron narrow trigger for  $Q^2 = 1.1$  (top) and  $Q^2 = 1.9$  (GeV/c)<sup>2</sup> (bottom).

## 435 5 Summary

436 A scaler-based counting DAQ with hardware-based particle identification was suc-  
 437 cessfully implemented in the 6 GeV PVDIS experiment at Jefferson Lab. Asymme-  
 438 tries measured by the DAQ follow Gaussian distributions as expected from purely

439 statistical measurements. Particle identification performance of the DAQ was mea-  
440 sured and corrections were applied to the data on a day-to-day basis. The overall  
441 pion contamination in the electron sample was controlled to approximately  $2 \times 10^{-4}$   
442 or lower, with an electron efficiency above 91% throughout the data production pe-  
443 riod of the experiment. The DAQ deadtime was evaluated from a full-scale timing  
444 simulation and contributes an approximately 0.2% uncertainty to the final asym-  
445 metry results. The systematic uncertainties from the pion contamination and the  
446 counting deadtime are therefore both negligible compared to the (3 – 4)% statis-  
447 tical uncertainty and other leading systematic uncertainties. Results presented here  
448 demonstrate that accurate asymmetry measurements can be performed with even  
449 higher event rates or backgrounds with this type of scaler-based DAQ.

## 450 Acknowledgments

451 This work is supported in part by the Jeffress Memorial Trust under Award No.  
452 J-836, the U.S. National Science Foundation under Award No. 0653347, and the  
453 U.S. Department of Energy under Award No. de-sc0003885. **Notice:** Authored  
454 by Jefferson Science Associates, LLC under U.S. DOE Contract No. DE-AC05-  
455 06OR23177. The U.S. Government retains a non-exclusive, paid-up, irrevocable,  
456 world-wide license to publish or reproduce this manuscript for U.S. Government  
457 purposes.

## 458 References

- 459 [1] JLab experiment E08-011 (previously E05-007), R. Michaels, P.E. Reimer and X.-C.  
460 Zheng, spokespersons.
- 461 [2] R. Subedi *et al.*, AIP proceedings of the 18<sup>th</sup> International Spin Physics Symposium  
462 (2009) 245.
- 463 [3] A publication about the E08-011 physics asymmetries is in preparation.
- 464 [4] K. Nakamura *et al.* [Particle Data Group], J. Phys. **G37**, 075021 (2010).
- 465 [5] J. Alcorn *et al.*, Nucl. Instrum. Meth. **A522** (2004) 294.
- 466 [6] R. Hasty *et al.* [SAMPLE Collaboration], Science **290**, 2117 (2000).
- 467 [7] K. A. Aniol *et al.* [HAPPEX Collaboration], Phys. Rev. C **69**, 065501 (2004).
- 468 [8] A. Acha *et al.* [HAPPEX Collaboration], Phys. Rev. Lett. **98**, 032301 (2007).
- 469 [9] K. A. Aniol *et al.* [HAPPEX Collaboration], Phys. Rev. Lett. **96**, 022003 (2006).
- 470 [10] K. A. Aniol *et al.* [HAPPEX Collaboration], Phys. Lett. B **635**, 275 (2006).

- 471 [11] Z. Ahmed *et al.* [HAPPEX Collaboration], Phys. Rev. Lett. **108**, 102001 (2012).
- 472 [12] S. Abrahamyan, Z. Ahmed, H. Albatineh, K. Aniol, D. S. Armstrong, W. Armstrong,  
473 T. Averett and B. Babineau *et al.*, Phys. Rev. Lett. **108**, 112502 (2012).
- 474 [13] C.Y. Prescott *et al.*, Phys. Lett. **B77** (1978) 347.
- 475 [14] C.Y. Prescott *et al.*, Phys. Lett. **B84** (1979) 524.
- 476 [15] F. E. Maas *et al.* [A4 Collaboration],  $Q^2 = 0.230-(\text{GeV}/c)^2$ ,” Phys. Rev. Lett. **93**,  
477 022002 (2004).
- 478 [16] F. E. Maas, K. Aulenbacher, S. Baunack, L. Capozza, J. Diefenbach, B. Glaser,  
479 T. Hammel and D. von Harrach *et al.*,  $Q^2 = 0.108 (\text{GeV}/c)^2$ ,” Phys. Rev. Lett.  
480 **94**, 152001 (2005).
- 481 [17] S. Baunack, K. Aulenbacher, D. Balaguer Rios, L. Capozza, J. Diefenbach, B. Glaser,  
482 D. von Harrach and Y. Imai *et al.*, Phys. Rev. Lett. **102**, 151803 (2009).
- 483 [18] D. H. Beck, Phys. Rev. D **39**, 3248 (1989).
- 484 [19] D. S. Armstrong *et al.* [G0 Collaboration], Phys. Rev. Lett. **95**, 092001 (2005).
- 485 [20] D. Androic *et al.* [G0 Collaboration], Phys. Rev. Lett. **104**, 012001 (2010).
- 486 [21] D. Marchand, J. Arvieux, G. Batigne, L. Bimbot, A. S. Biselli, J. Bouvier, H. Breuer  
487 and R. Clark *et al.* Nucl. Instrum. Meth. A **586**, 251 (2008).
- 488 [22] D. Androic *et al.* [G0 Collaboration], Nucl. Instrum. Meth. A **646**, 59 (2011).